Mon. Not. R. astr. Soc. (1974) **169,** 607–629.

HIGH RESOLUTION OBSERVATIONS OF NEUTRAL HYDROGEN IN M31—I.

The Overall Distribution

D. T. Emerson

(Communicated by J. E. Baldwin)

(Received 1974 June 27)

SUMMARY

Observations of the galaxy M31 at 21 cm wavelength have been made with the Cambridge Half-Mile telescope, enabling the neutral hydrogen to be mapped with an angular resolution of $1'{\cdot}5 \times 2'{\cdot}2$ and a velocity resolution of 39 km s^{-1}. The central deficiency of H I is found to extend to 4 kpc from the nucleus but beyond that distance the H I emission is seen to be strongly associated with dust lanes. The surface densities of H II regions and the youngest OB associations are found to vary approximately as the square of the H I surface density. H I emission along the major axis has been detected to 162′ (32·4 kpc) SW from the nucleus, and to 120′ (24 kpc) NE.

1. INTRODUCTION

Several surveys of the neutral hydrogen in M31 have been published (Burke, Turner & Tuve 1963, 1964; Argyle 1965; Roberts 1966; Davies & Gottesman 1970; Guibert 1974), the highest angular resolution employed until now being 10 arcmin ($\equiv 2{\cdot}0$ kpc along the major axis, if the distance of M31 is taken as 690 kpc) by Roberts. The main features of the hydrogen distribution revealed by these studies are as follows:

(i) An overall ring-like structure of radius 10 kpc, coincident with the main ring of H II regions.

(ii) Peaks in the H I distribution along the major axis identified with spiral arms traced by H II regions.

(iii) A low central density; within 2 kpc of the nucleus the upper limit to the projected H I density is ≈ 15 per cent of that at the peak of the ring (Guibert 1974).

(iv) Peak brightness temperatures of 24 K for a 10′ arc beam and a 20 km s^{-1} velocity resolution (Roberts 1966), and 30 K for a $14' \times 18'$ arc beam and 8·4 km s^{-1} velocity resolution (Davies & Gottesman 1970).

(v) The so-called SW companion (Burke *et al.* 1963), an H I feature about 2° from the nucleus along the major axis, linked with the main part of the galaxy by a bridge of H I (Davies & Gottesman 1970).

The present observations (Emerson 1972) are of higher angular resolution ($1'{\cdot}5 \times 2'{\cdot}2$ arc) and consequently reveal further details. They are described in two papers, of which this deals primarily with the general features of the distribution of H I, and the second with the velocity field. New information is presented here on the ‘ ring ’ structure and its detailed relation to the optical and radio continuum features is established for the first time.

2. THE OBSERVATIONS AND REDUCTION OF DATA

The observations were made with the Cambridge Half-Mile telescope, using the techniques described by Baldwin *et al.* (1971). The total extent of H I along the major axis of M31 is $\sim 5°$; three separate surveys were therefore necessary for mapping this galaxy with the Half-Mile telescope, and Fig. 1 shows the three positions of the half-power response of the primary beam, superposed on the outermost contour of the neutral hydrogen detected by Davies & Gottesman (1970).

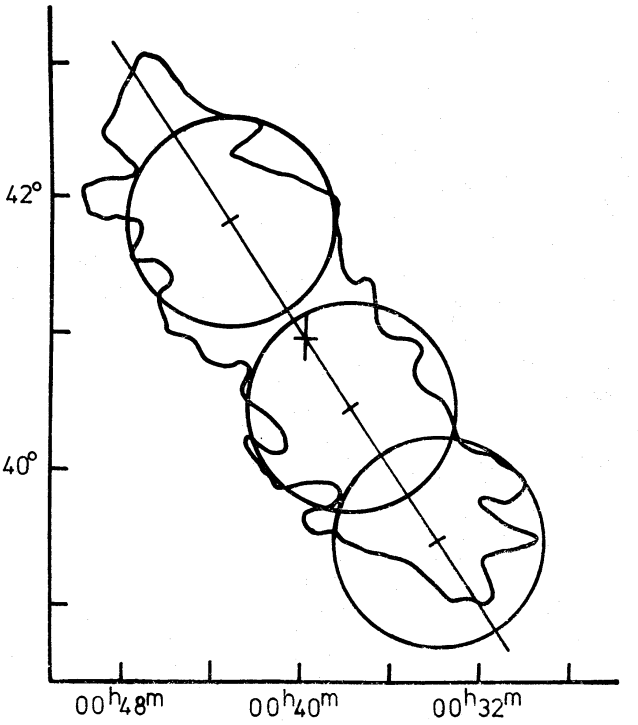

FIG. 1. *The positions of the three separate surveys made of M31, superposed on a contour showing the limit of the neutral hydrogen detected by Davies & Gottesman* (1970).

Here, and elsewhere in the paper, position coordinates are for epoch 1950·0. Twelve-hour observations at each of 60 spacings were made for the two surveys covering the main part of the galaxy, and at 15 spacings for the extreme SW survey. The equipment was that used for the observations of M33 (Wright, Warner & Baldwin 1972; Warner, Wright & Baldwin 1973) with a velocity resolution of 39 km s^{-1}, although the system noise was improved to 120 K. Table I summarizes the parameters of the surveys, which were calibrated with respect to the continuum sources 3C 345 and 3C 286 whose flux densities at 1421 MHz were taken to be 6·6 and $7{\cdot}45 \times 10^{-26}$ W m^{-2} Hz^{-1} respectively.

As in the case of M33, the observations were reduced to give maps of:

(i) the H I emission within velocity ranges of width 39 km s^{-1} centred on radial velocities separated by 26 km s^{-1};

(ii) the integrated H I emission; and

(iii) the radial velocity of the H I at those points where the spectra may be represented adequately by a single value of velocity.

Only those features of the analysis which differ from those described by Baldwin *et al.* (1971) are noted.

TABLE I

Survey	Mean epoch of survey	Map centre of survey (1950·0) RA h m s	Decl. ° ′	Angular resolution	Sensitivity rms noise level in 38 km s^{-1} velocity range
North	1970·7	00 43 30	41 50	6′·0 × 9′·0	0·2 K ≡ 0·05 fu per beam area
	1971·0			90″ × 135″	1·5 K ≡ 0·025 fu
Middle	1970·0	00 38 00	40 30	6′·0 × 9′·2	0·25 K ≡ 0·06 fu
	1970·2			90″ × 139″	2·0 K ≡ 0·03 fu
South	1970·8	00 34 00	39 30	6′·0 × 9′·4	0·2 K ≡ 0·05 fu

The smallest feasible separation of the 9-m paraboloids is about 60 λ, so that structure on a scale larger than ∼1° could not be observed. To correct for the resulting variations of zero level across the maps of H I emission, the amplitudes of the missing spatial frequencies were numerically filtered from data with comparable velocity resolution (35 km s^{-1}) kindly made available by Argyle from his work in 1965; these frequencies were then added to the data obtained in the present survey. Spurious large-scale features remaining after this correction procedure (described in detail by Emerson 1973) have brightness temperatures of ∼0·5 K, comparable in magnitude to the noise level of the maps of resolution 6′ × 9′ (Table I) and less than the noise level of the maps of higher resolution.

The positional accuracy of the surveys has been checked by comparison with sources in the 5C 3 survey of the same area (Pooley 1969) and the agreement is within 10″ arc in all cases.

The sensitivity to low brightness H I emission in a particular direction can be improved by integrating the emission over velocity channels which are known to contain H I emission, but omitting those which do not. In the present work, only those channels at each map grid-point with contributions exceeding 2·5 × the rms noise level were included in the integration. The disadvantage of this technique is that low brightness H I emission occurring over a wide range of velocities is underestimated; this does not lead to any serious error.

Except near discrete sources the brightness of 1421 MHz continuum emission from M31 (typically ∼0·3 K) is much less than the H I brightness. However, the H I data were corrected for this continuum contribution by means of observations made with a broadband receiver in parallel with the line receiver.

3. LARGE SCALE FEATURES OF THE H I DISTRIBUTION

Plate I shows the integrated H I emission at a resolution of 6′ × 9′ arc, superposed on an optical photograph. The sensitivity to extended regions of low brightness temperature is greater than in the high resolution (1′·5 × 2′·2) maps which are described later. The following features are apparent:

(i) The large overall extent of the H I emission along the major axis; emission can be detected to 120′ (24 kpc) NE of the nucleus, and to 162′ (32·4 kpc) SW—the latter is visible with a brightness of ∼0·8 K on maps with a limited velocity range, but is below the level of the first contour of integrated emission in Plate I.

For comparison, the limiting brightness of $26^{m}\cdot8$ (arcsec)$^{-2}$ in the B photometry by de Vaucouleurs (1958) occurs at distances of $\pm 123'$ from the nucleus along the major axis.

(ii) The H I emission from the NE half of the ' ring ' is brighter than from the SW half. This has been noted by previous observers.

(iii) The ' SW Companion ' at the end of the major axis, $\approx 2°$ from the nucleus. The bridge between this and the main part of the galaxy is clearly visible in Plate I.

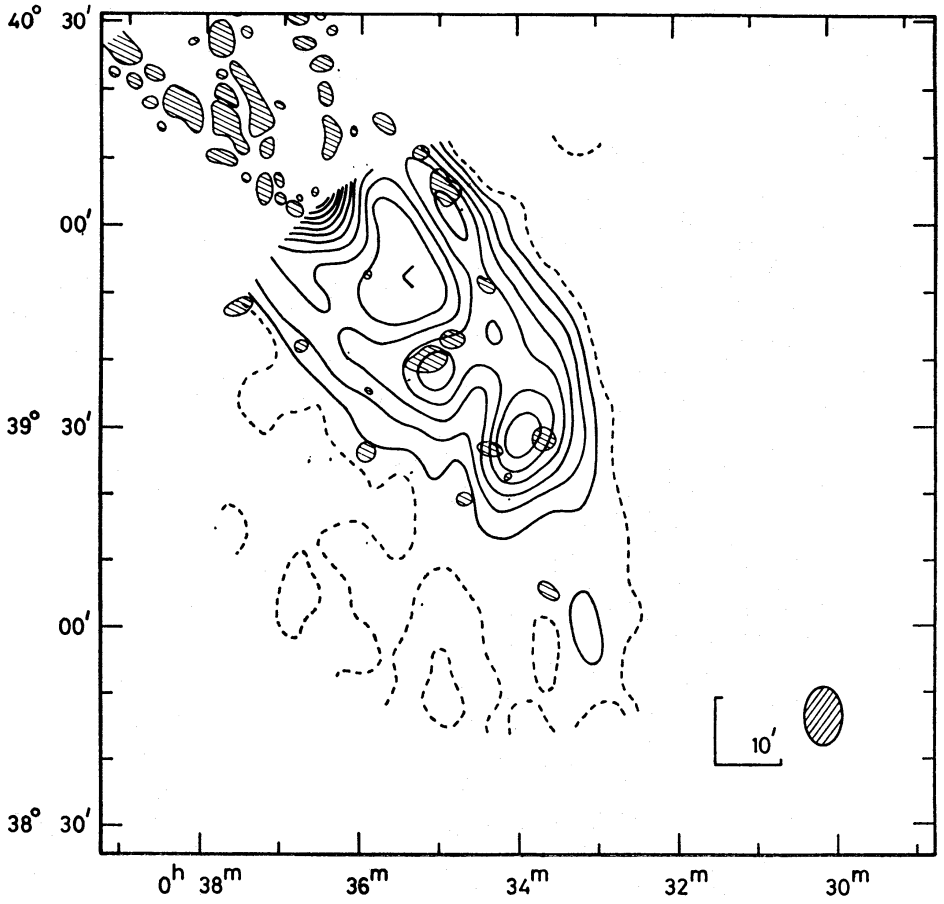

FIG. 2. *Integrated H I emission and OB associations in the extreme South of M31. The OB associations, shown shaded, are from van den Bergh* (1964) *and from Richter* (1971). *The contour interval is* 100 *K km s*$^{-1}$, *the first non-zero contour being dotted.*

Fig. 2 shows the region in more detail, together with the positions of the OB associations found by van den Bergh (1964) and by Richter (1971); these are seen to be related to the H I distribution. A bridge to the main galaxy is also found in H I on the SE side of the major axis at $\alpha = 00^{h}\,36^{m}\cdot5$, $\delta = 39°\,45'$ and there can be little doubt as to the close relationship of the SW companion with the main part of M31. It is part of an outer arm which, at higher resolution, can be traced as a continuous feature along the SE edge of M31, passing through the possible companion ' Andromeda IV ' found by van den Bergh (1972) and discussed in Section 5.2.

(iv) The central deficiency previously reported by many authors is clearly seen in Plate I, although it is still not quite resolved along a direction parallel to the minor axis.

In order to obtain the best sensitivity to H I emission in this central region, whilst keeping the maximum available resolution in the minor axis direction, the following procedure was adopted. The maps of individual velocity channels at high angular resolution were each smoothed in a direction parallel to the major axis, so that the effective beam shape becomes elliptical with approximately the same axial ratio as M31; these maps retain the full angular resolution across the minor axis of M31 but the noise level is reduced by a factor of 3. They were then combined

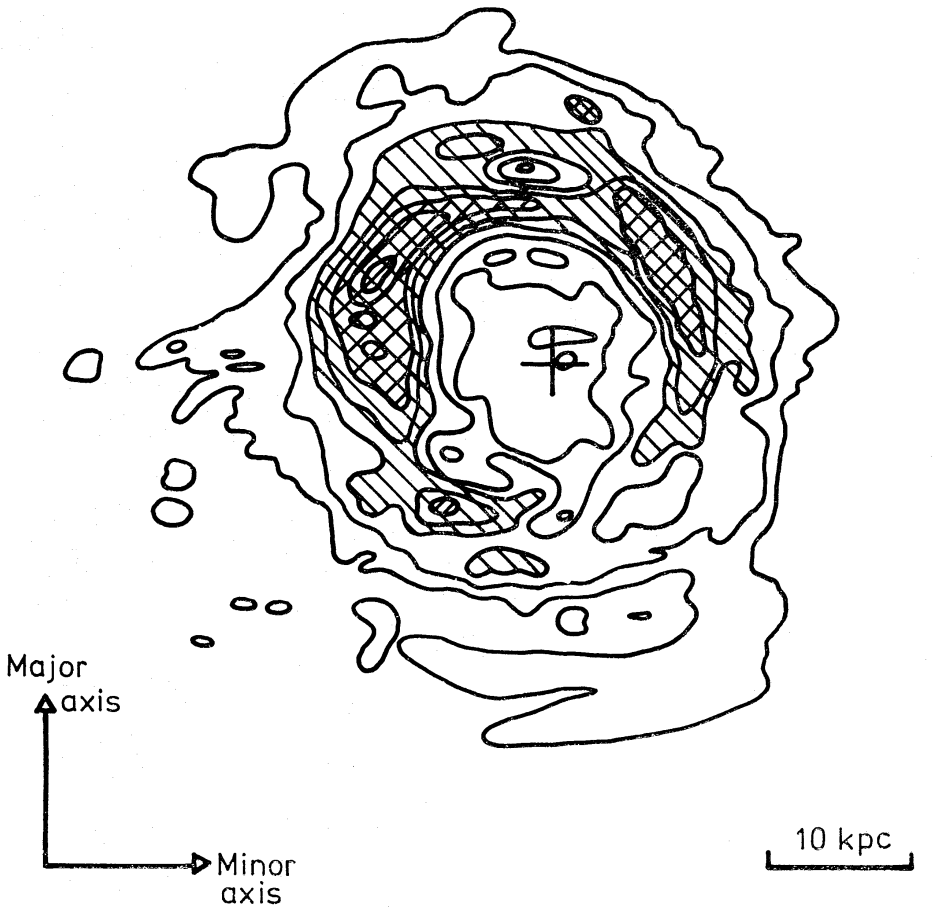

FIG. 3. *A rectified map of the H I distribution in M31, made with a beam shape which would appear circular projected on to the plane of the galaxy, with half-power width of 1800 pc. The data from the M31 'South' survey are also included, which has poorer resolution parallel to the minor axis. The contour interval is in units of 400 K km s^{-1} for H I emission observed along the line of sight and is not corrected for the inclination of M31.*

as described in Section 2 to give a more sensitive map of integrated H I emission than is obtained with the original high-resolution data; this is shown in Fig. 3, rectified to give a 'face-on' view of the galaxy. Faint H I emission is seen close to the nucleus; some of this H I has 'normal' velocities (Emerson & Baldwin 1973) but some, within 5′ of the nucleus, has anomalous velocities. The latter will be described in Paper II.

Emerson & Baldwin found brightness temperatures of ~ 3 K along the NE major axis within 20′ of the nucleus; allowing for beam smoothing, this would correspond to a surface density normal to the plane of M31 of $(10 \pm 3) \times 10^{19}$ atom cm^{-2}. (The projected density along the line of sight, assuming the gas to be optically

thin, is taken as $N_H = 1{\cdot}82 \times 10^{18} \int T_b \, dV \, \mathrm{cm}^{-2}$, where T_b is the observed H I brightness temperature and V is the radial velocity in kilometres per second (km s^{-1}). The inclination of the plane of M31 is taken as 78°.) In the present survey such a density would just have escaped detection away from the major axis in this central region, since it would have been received at low brightness smeared over a number of adjacent spectrometer channels. It is thus likely that the surface density of $\sim 10^{20}$ atom cm^{-2} extends over the entire central region of M31. This

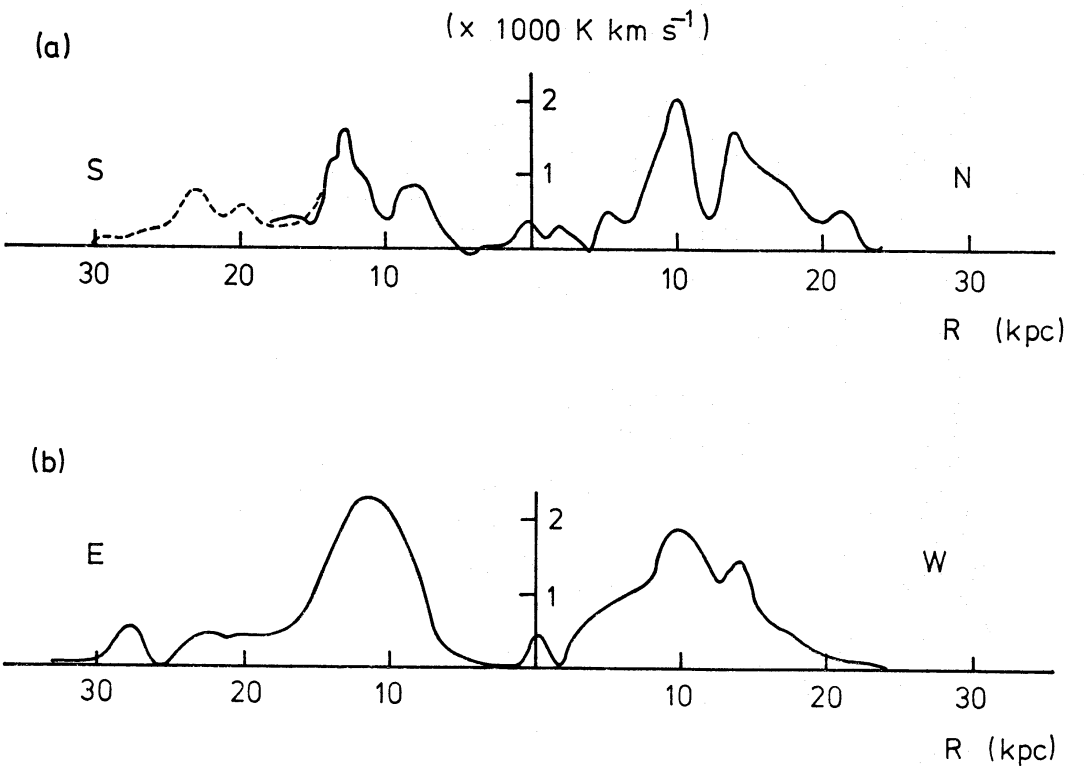

FIG. 4. *Cuts from Fig. 4 along the major and minor axes of M31, showing the projected H I density as a function of radius in the galaxy.*

value is in good agreement with the estimate made by Guibert (1974) from model-fitting of his data, that the surface density in this region lies between 6·5 and 14×10^{19} atom cm^{-2}. Apart from a small amount of dust, the central region contains mainly old stars and Population II objects, so the low density of H I is not unexpected.

Fig. 4 shows cuts from Fig. 3 along the major and minor axes of M31; the linear resolution along both axes is identical ($\approx$ 1·8 kpc hpbw) if the galaxy can be represented by a flat, thin disc. Adjacent H I arms are seen to be well separated along the major axis, but are confused along the minor axis. Two factors may contribute to this confusion:

(i) The H I distribution has a finite thickness; a thickness of $\sim$ 500 pc (somewhat greater than is found at a comparable radius in our own Galaxy) would account for a large part of the observed effect.

(ii) The spiral pattern is distorted, in particular along the SE minor axis; this distortion is observed in the distribution of H II (Arp 1964) and OB associations (van den Bergh 1964) as well as in H I, and is probably attributable to the companion

galaxy M32. The effect of the distortion is to reduce the apparent separation of adjacent arms.

Fig. 5 shows a map of the peak brightness temperatures of H I. Such a map is probably a more useful guide to the H I spiral structure than maps of integrated emission since emission profiles in the interarm regions are very often double-humped as a result of confusion (caused by line-of-sight and beam-smearing effects) between adjacent arms with different radial velocities. Whereas both peaks in the profile contribute to the maps of integrated emission, only the stronger peak contributes to the map of peak brightness, and adjacent arms are thus more easily separated in the latter than in the former.

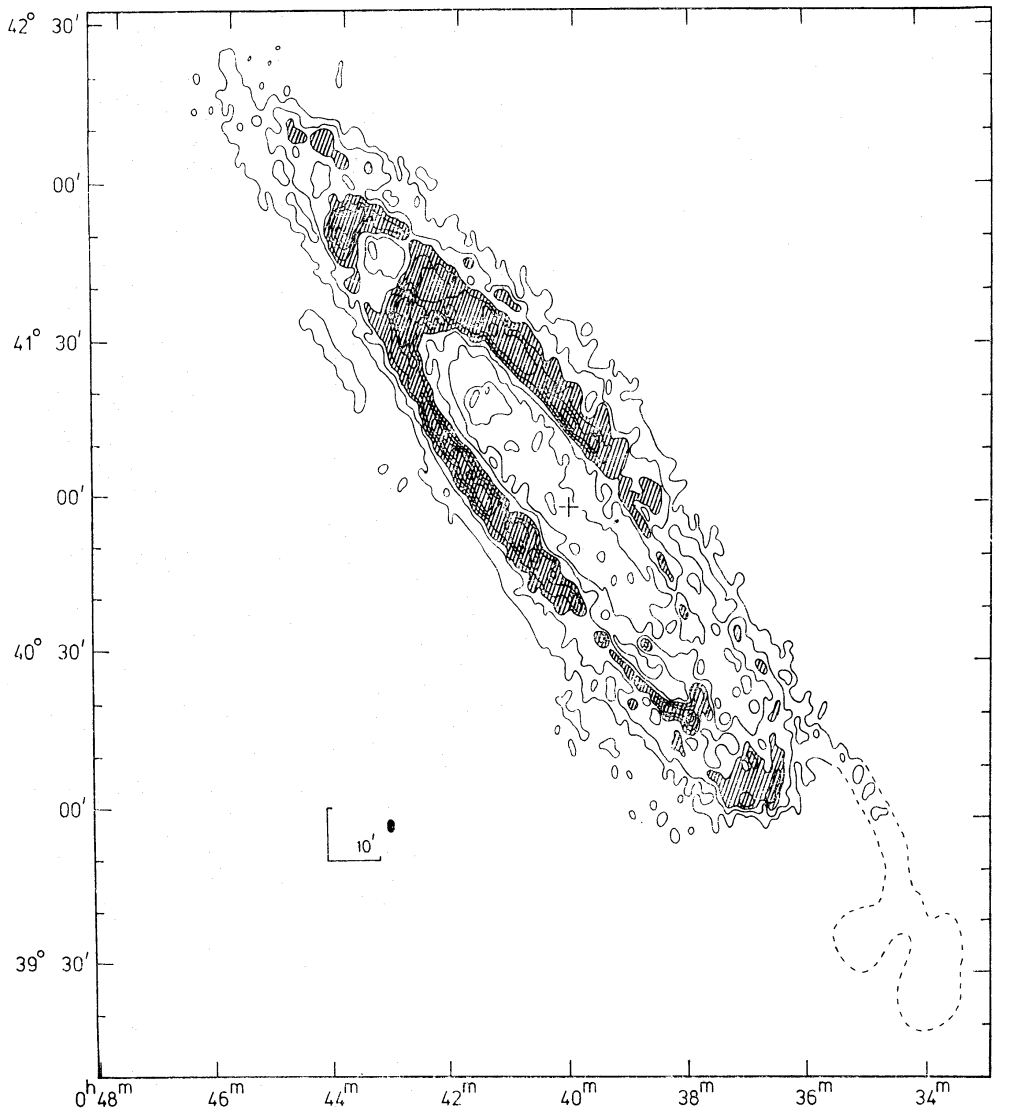

FIG. 5. *Peak brightness temperatures of H I emission observed within a 39 km s^{-1} velocity range. This is a composite map made from the high resolution M31 'North' and 'Middle' surveys, with a single contour from the M31 'South' survey at lower resolution shown dotted. The contour interval is 8 K, with regions brighter than 24 K shown shaded. The rms noise level is ~2 K near the map centre of each high-resolution survey, increasing to ~4 K at the half-power points of the primary beams.*

The nucleus of M31 is marked with a cross.

It is not possible from the H I structure observed in M31 to distinguish between leading and trailing spiral arms. This ambiguity results from:

(i) the high inclination of the plane (78°) and the line-of-sight confusion along the minor axis; and

(ii) the near-circularity of the 'spiral' arms (pitch angle $< 10°$) and the importance of even small distortions in the spiral structure. These factors are

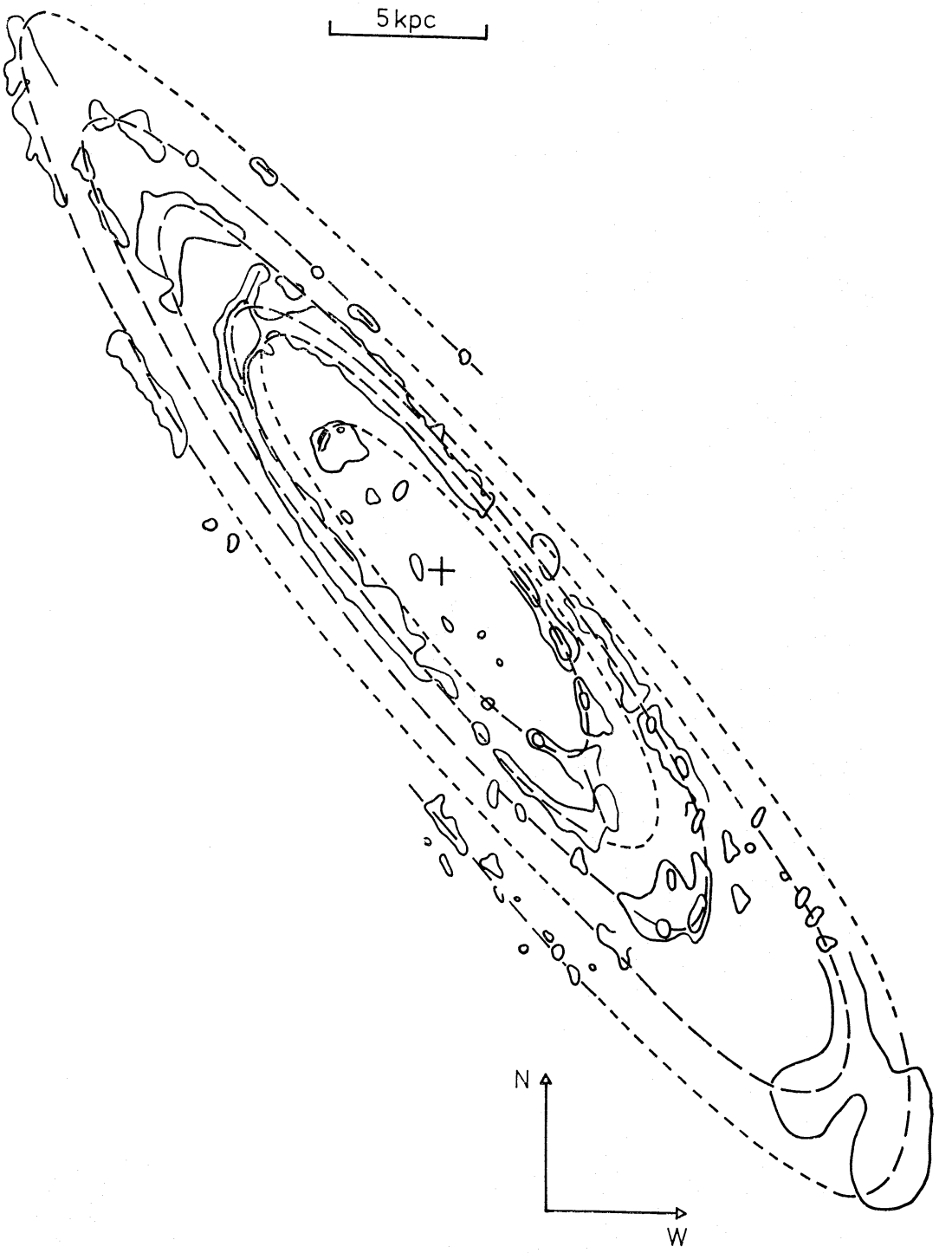

FIG. 6. *Peak contours from Fig.* 6, *with a suggested interpretation* (*an 'artist's impression'*) *of the H* I *structure in M31 in terms of a two-armed trailing spiral.*

intrinsic to M31 and it is unlikely that future H I observations, even with improved angular resolution and signal-to-noise ratio, will enable its spiral structure to be determined uniquely.

With the assumption that M31 is composed of a two-armed trailing spiral, Fig. 6 shows a possible interpretation of the observed H I spiral structure.

4. THE DETAILED DISTRIBUTION OF H I, AND ITS RELATION TO OTHER POPULATION I MATERIAL

This section discusses details of the H I distribution revealed by the maps with high angular resolution ($1\frac{1}{2}' \times 2'$), in particular its relationship with dust, H II regions, OB stars, and radio continuum radiation.

4.1 *H I and dust*

Plate II(a) and (b) show contour maps of the integrated H I emission superposed on an optical print of M31. The two halves of the galaxy have been kept separate in these maps, owing to the difficulty of matching the scales to sufficient accuracy over the large area of sky involved. A striking feature is the correlation of peaks of H I emission with dust lanes, most apparent towards the southern limit of optical emission in Plate II(b) where the dust is easily seen. The resolution along the major axis is ≈ 350 pc in the plane of M31 and the peaks of H I coincide with the centres of the dust clouds to within about 100 pc. Many H I ridges can be traced running along dark dust lanes. The correlation is not obvious, however, where the lanes cross the minor axis; this results from the confusion of adjacent H I arms along the minor axis. The strongest correlation of H I with dust is found between 4 and 12 kpc from the nucleus. In this region there is usually a prominent dust feature wherever there is a peak in the H I distribution. Within 4 kpc, however, some dust is seen—for example the prominent dust lane along the NW edge of the bright nuclear bulge—but little H I. This is consistent with the central deficiency of H I mentioned in the previous section, but it should be noted that dust is particularly easy to detect in this region on account of the bright background, and the actual mass of dust involved may be relatively small. Beyond the areas of bright optical emission ($R \gtrsim 12$ kpc), the H I features do not appear to correspond with dust. This may be due merely to the difficulty of detecting the dust here and it is entirely possible that dust and H I are in fact co-existent in these regions but the dust cannot be seen.

4.2 *H I and H II regions*

Fig. 7(a) and (b) show the H I distribution together with the positions of H II regions from Baade & Arp (1964). The general agreement is seen to be very good and regions of strong H I emission tend to be associated with clusters of H II regions. On scales of less than 1 kpc, however, there appears to be an anti-correlation of H I and H II, with H II regions clustered around a peak of H I emission rather than coincident with it. This relative displacement of H I peaks and H II regions cannot be explained by beam-smoothing effects on the observed H I distribution, and is an order of magnitude greater than the maximum positional uncertainties of the observations. It is probably due to the obscuration of H II regions by the dust which is associated with the high H I density. Mezger (1969) has concluded that the optically observed H II regions in our own Galaxy have a

distribution determined by the extinction effects of interstellar dust; owing to the high inclination of the plane of M31, interstellar extinction is likely to affect the apparent distribution of H II regions there also. If H II regions are indeed present within the dust lanes, they could perhaps be detected by their centimetric radio emission.

In order to quantify the correlation a histogram of the surface density of H II regions within different ranges of integrated H I emission has been plotted (Fig. 8).

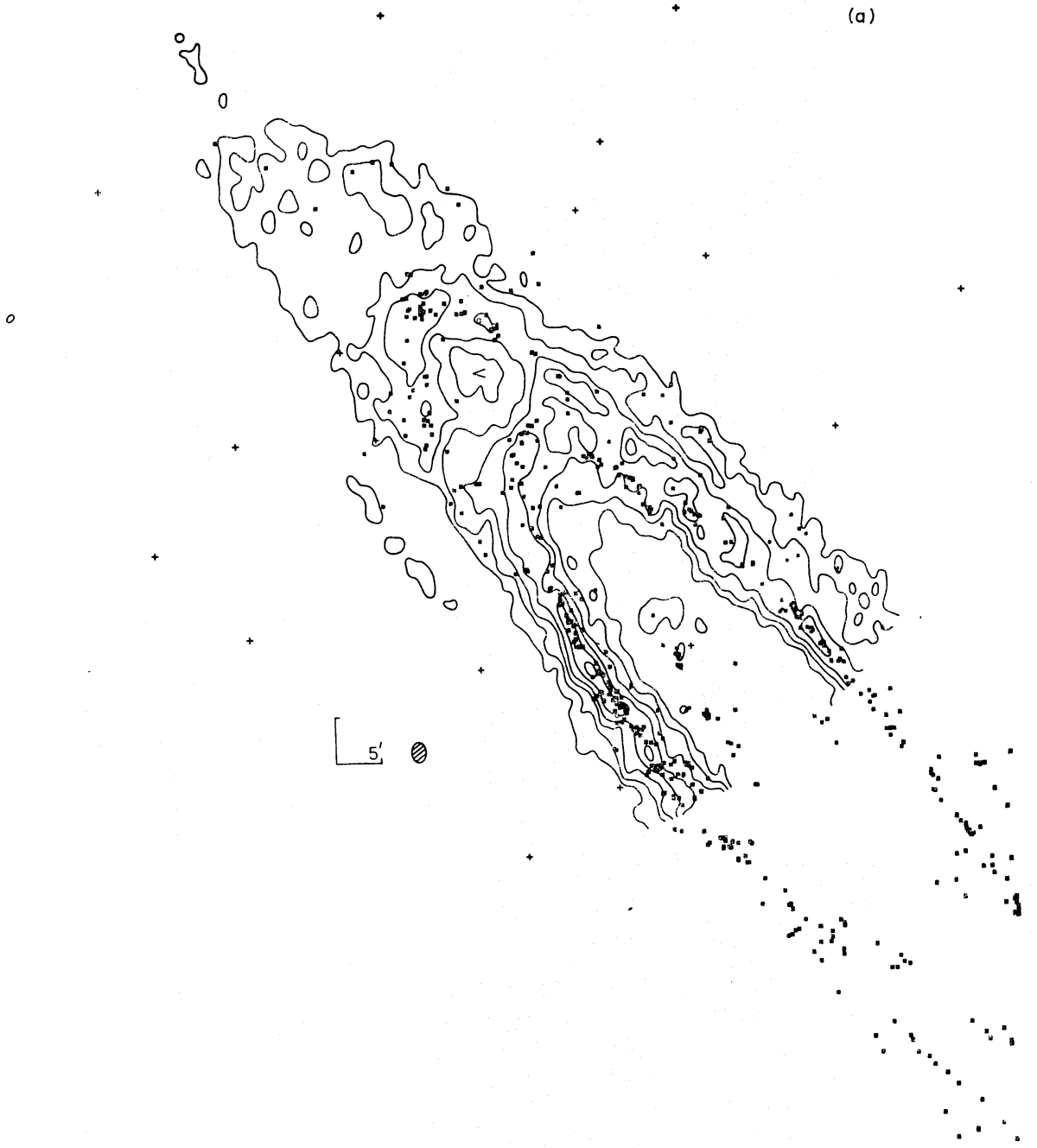

FIG. 7. *Integrated H* I *emission and H* II *regions in M31. The dots represent H* II *regions catalogued by Baade & Arp* (1964) *and are shown superposed on a contour map of integrated H* I *emission. The contour intervals and noise levels are as in Plate II and the North* (*a*) *and South* (*b*) *halves of the galaxy are, as before, shown separately.*

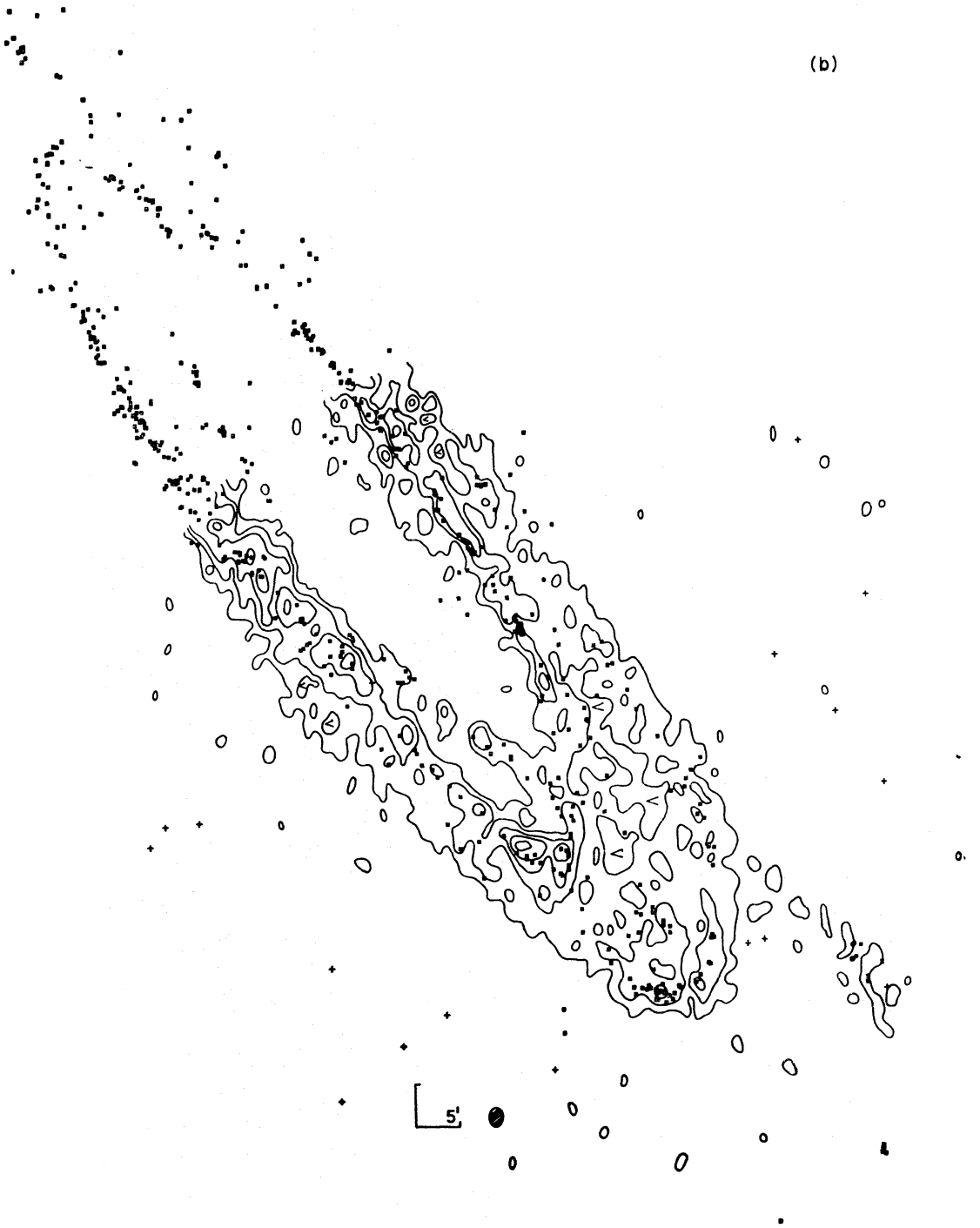

FIG. 7(b)

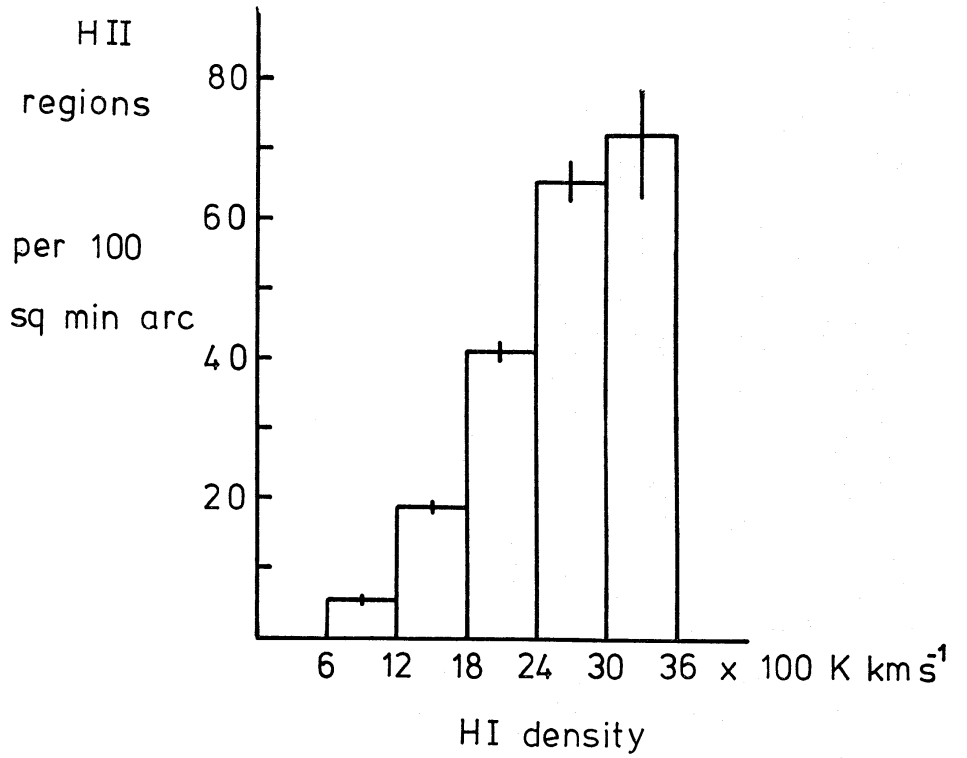

FIG. 8. *Projected densities of H* II *regions against observed H* I *emission in M31. The error bars indicate the statistical uncertainty σ; the H* II *density in regions of H* I *emission* < 600 *K km s*$^{-1}$ *is* $0{\cdot}67 \pm 0{\cdot}08$ *per* 100 *sq. min arc (see text).*

To obtain the value for H II density in the lowest range of H I density (< 600 K km s^{-1}), the outermost limit of H I emission around M31 has been arbitrarily taken as the 200 K km s^{-1} contour from the lower-resolution ($6' \times 9'$) data of Plate I. It is seen from this histogram that there is little increase of the density of H II regions with H I density above ~ 3000 K km s^{-1}; this is a manifestation of the anti-correlation of H I and H II regions on a scale of ~ 100 pc which was discussed above.

Fig. 8 suggests that a law of the form: $(\sigma_{\mathrm{H\,II}}) \propto (\sigma_{\mathrm{H\,I}})^n$ may be appropriate. From a plot (Fig. 9) of log (H II surface density) against log (H I surface density), n is found to be $2{\cdot}23 \pm 0{\cdot}11$, which may be compared with the value $n = 3{\cdot}50 \pm 0{\cdot}12$ obtained by Hartwick (1971) from a similar analysis of Roberts' data. The apparent discrepancy is due entirely to the different scale sizes over which Roberts' survey and the present observations have averaged the H I density; Roberts' beam was 2×9 kpc in the plane of M31, whereas the beam in the present survey is 350×1800 pc. This value for the index n is in agreement with what is known about the Magellanic Clouds (Sanduleak 1969) and our own Galaxy (Schmidt 1959) from H I data with comparable linear resolution. The linear scale over which data are averaged is clearly an important factor to be considered in such comparisons.

4.3 *H* I *and OB associations*

Fig. 10(a) and (b) show contours of the integrated H I emission superposed on the positions of OB associations listed by van den Bergh (1964) and it is seen that there is excellent general agreement between lines of OB associations and ridges of H I emission. The beam-size of the H I observations, 350×1800 pc in the plane of

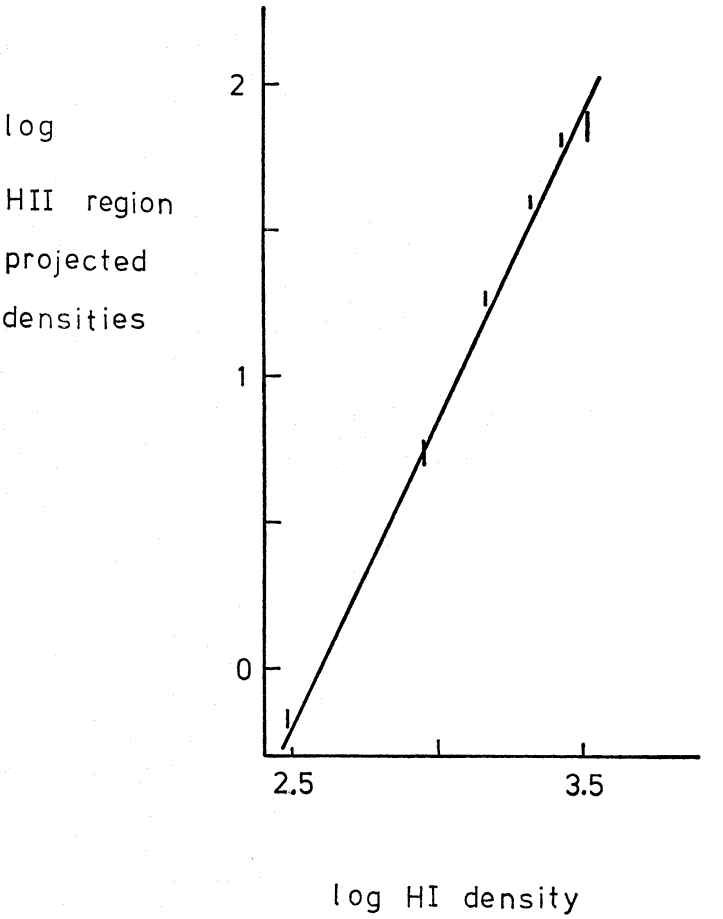

FIG. 9. *The H II and H I densities from Fig. 8 plotted logarithmically.*

M31, is comparable to the sizes of individual associations, which range from 300 pc for young to 800 pc for old associations. A comparison of the distribution of OB associations with the low-resolution map of Plate I, which is more sensitive to H I emission of lower brightness, shows that at least 186 of the 188 associations listed by van den Bergh lie within a region of integrated H I emission brighter than 200 K km s^{-1} ($0{\cdot}8 \times 10^{20}$ atom cm^{-2} surface density in the plane of M31). The two possible exceptions are OB12 and OB188, in van den Bergh's notation. OB12 is only 3 kpc from the nucleus and is thus within the central region where there is a deficiency of H I. OB188 is 25 kpc from the nucleus, just at the limit of detected H I emission. The correlation between OB associations found by Richter (1971) and the H I projected density at the SW end of the major axis has already been confirmed in Section 3 (see Fig. 2). There is thus good general agreement, on scales of several hundred parsec to a few kiloparsec, between lines of OB associations and ridges of H I emission.

The correlation was investigated further in terms of estimated stellar densities by counting on Fig. 10(a) and (b) the number of van den Bergh's OB associations per unit area as a function of H I density. The number of stars in an individual OB association was assumed to be proportional to its linear extent along the major axis of M31 as measured by van den Bergh. If a particular OB associated was found to be divided nearly equally by one or two separate H I contours, it was arbitrarily

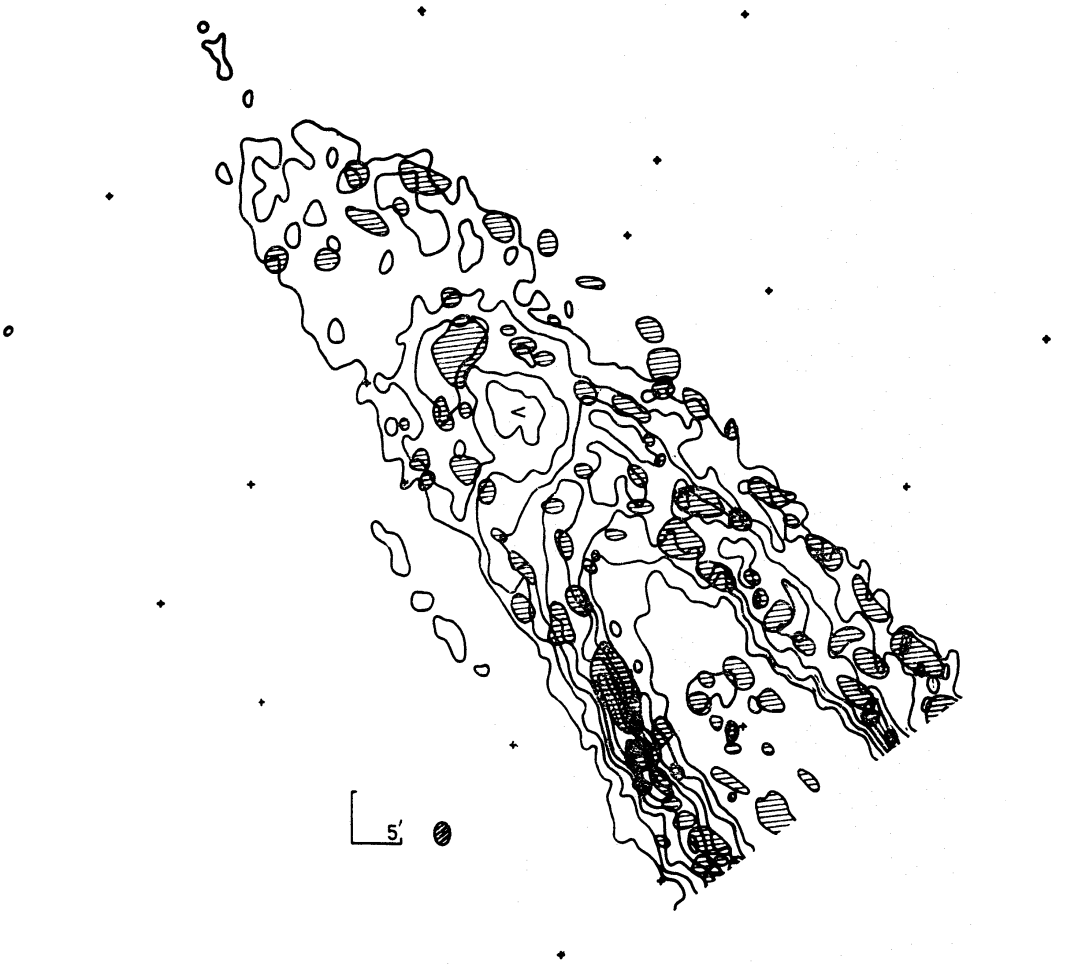

FIG. 10(a)

FIG. 10. *Contours of the integrated H* I *emission in M*31 *shown superposed on OB associations (shown shaded) catalogued by van den Bergh* (1964). *The contour interval is, as before,* 600 *K km* s^{-1}, *except in the south of (b), where the dotted contours are from the lower resolution M*31 *' South ' survey, and represent* 400 *K km* s^{-1} *and* 600 *K km* s^{-1}.

treated as two or three separate regions of equal weight. Associations listed by Richter have not been included in this analysis, since only the low resolution ($6' \times 9'$ beam) data are available for the extreme SW of M31. Shown in Fig. 11(a), (b), (c), (d) and (e) are the distributions for associations of different ages, as classified by van den Bergh.

Fig. 11(a) and (b) both indicate the high correlation of the density of OB stars and H I emission. The intermediate age ($\sim 30 \times 10^6$ yr) associations (Fig. 11(c)) reveal a much more limited correlation, while the old ($\sim 40 \times 10^6$ yr) associations (Fig. 1(d)) and those not classified according to age (Fig. 11(e)) show no significant correlation with H I densities—in particular, no old associations are found in regions of H I emission > 1800 K km s^{-1}. From the plots of Fig. 13(d) and (e) it may be inferred that those associations not classified by van den Bergh according to age are probably ' old '. Most of them are described as consisting of faint stars, which would be expected for older associations. Van den Bergh's age classification was based on the ' clumpiness ' of each individual association, combined with the mean size of

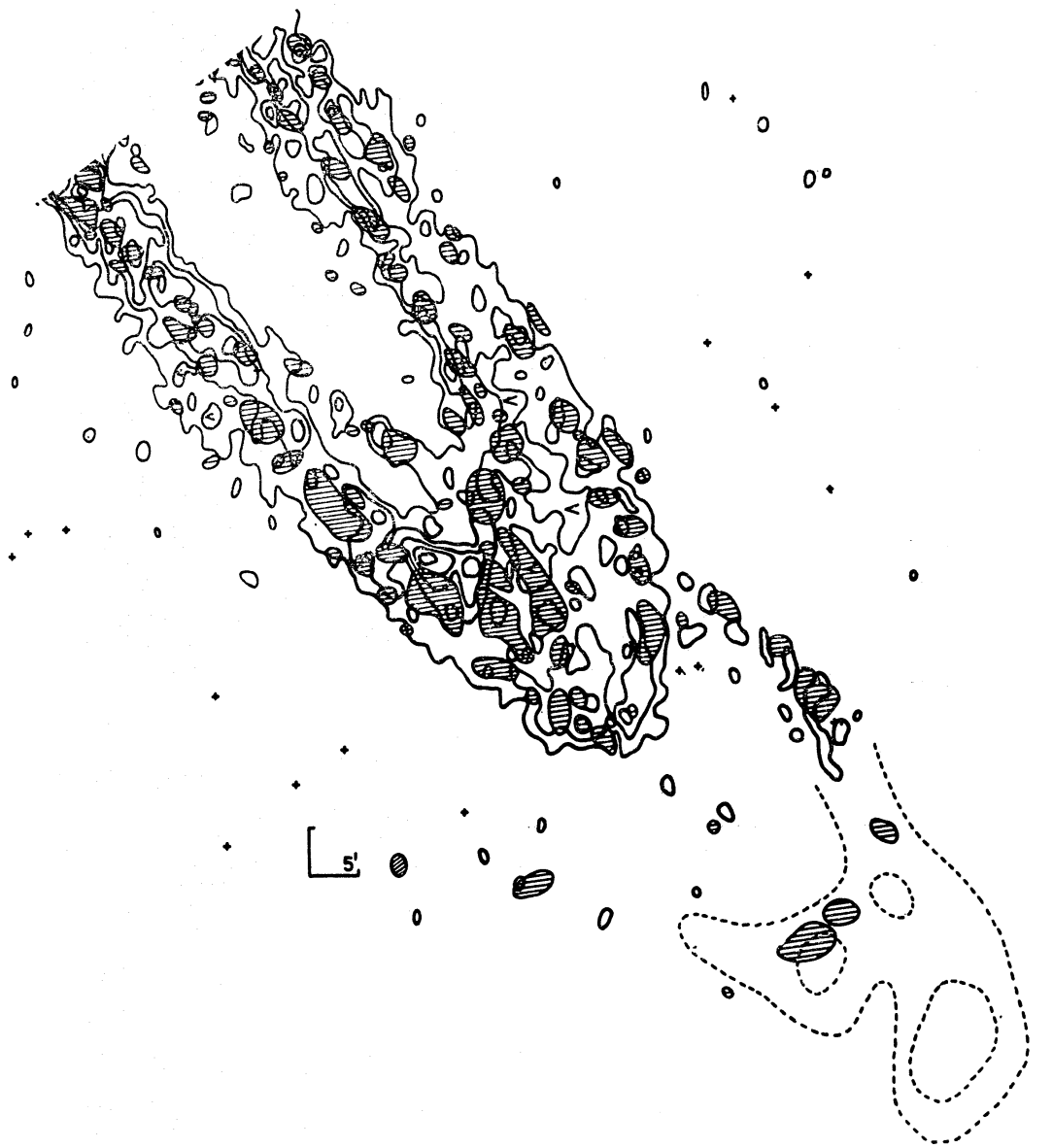

FIG. 10(b)

associations in each separate age group, and is therefore independent of the brightness of stars within the associations.

If the relation between estimated surface densities of OB stars and H I is assumed to be of the form: $(\sigma_{OB}) \propto (\sigma_{H\,I})^m$ where σ represents the surface densities respectively of OB stars and of H I, then the index m can be measured from a log–log plot of the two densities. Fig. 12 gives two such plots, one for the entire OB population, and one for those associations classified as ' young ', while in Table II are the computed slopes of these and similar plots both for OB associations of other ages and also for H II regions. It is seen that the younger the age of the objects, the greater the value of m. No value for m is included for the ' old ' associations, since there are too few of these for it to be meaningful, but the ' unclassified ' regions are considered to represent ' old ' associations.

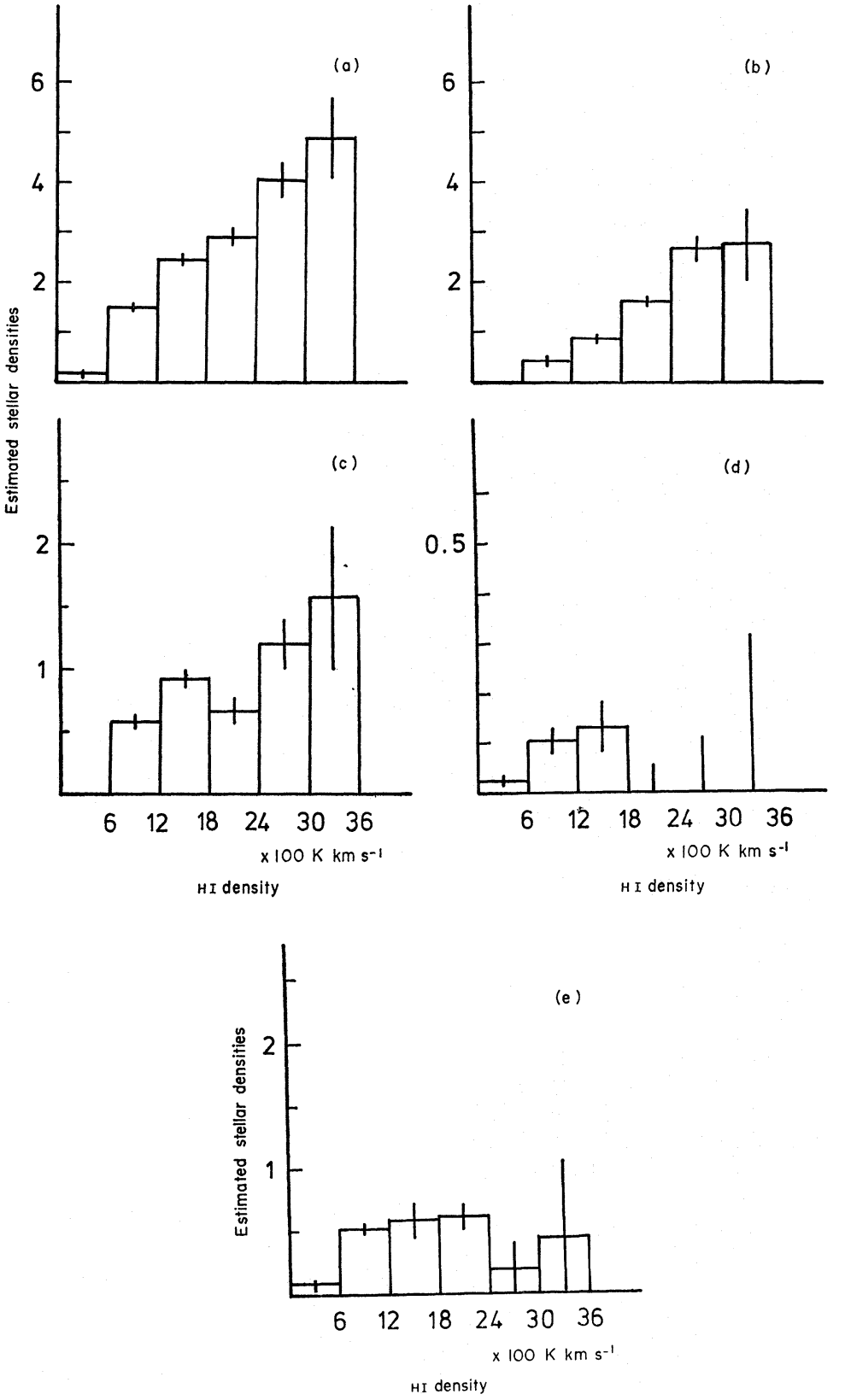

FIG. 11. *Estimated surface densities of OB stars of different ages against H* I *density.* (*a*) *All OB associations.* (*b*) *Young associations* ($1{\cdot}5 \times 10^7$ *yr*). (*c*) *Associations of intermediate age* (3×10^7 *yr*). (*d*) *Old associations* (4×10^7 *yr*). (*e*) *Associations not classified according to age by van den Bergh. The estimated stellar density in regions of H* I *emission* < 600 *K km s*$^{-1}$ *is too small to be shown clearly in the above plots. The values obtained are* (*a*) $0{\cdot}19 \pm 0{\cdot}02$, (*b*) $0{\cdot}044 \pm 0{\cdot}014$, (*c*) $0{\cdot}042 \pm 0{\cdot}011$, (*d*) $0{\cdot}020 \pm 0{\cdot}005$, (*e*) $0{\cdot}082 \pm 0{\cdot}014$. *The units of estimated stellar density are arbitrary.*

TABLE II

The dependence of the surface density of H II regions and OB associations on the projected H I density is assumed to be of the form:

$$\sigma_{OB} \text{ or } \sigma_{HII} \propto (\sigma_{HI},)^{m \text{ (or } n)}$$

σ is the surface density of OB stars, H II regions or H I.

Object	m (or n)	Standard error
All OB associations	0·87	0·07
Young associations	1·73	0·08
Intermediate age associations	0·77	0·26
Old associations	—	
Unclassified (=Old?)	0·13	0·17 (i.e. no correlation)
H II regions	2·23	0·11

The results found from the comparisons of OB associations and the H I distribution may be summarized as follows:

(i) There is a strong correlation of H I with OB associations, taking all ages of OB stars.

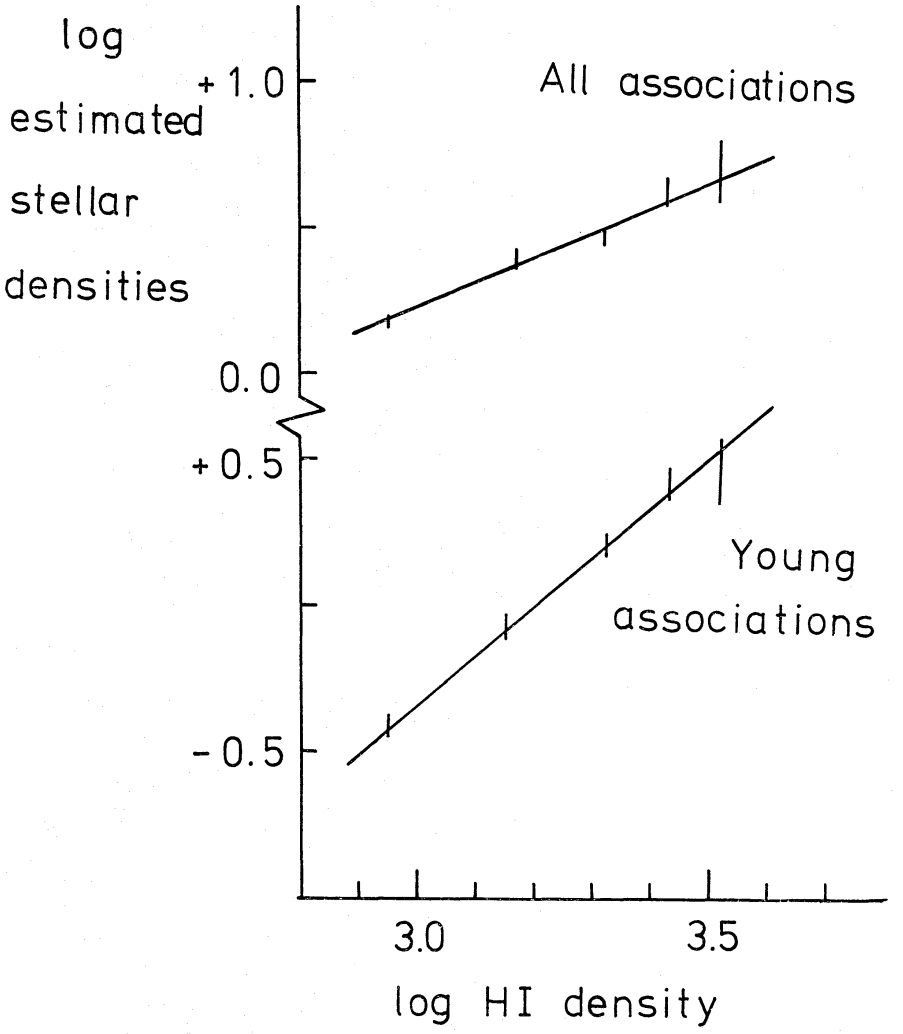

FIG. 12. *Surface densities of all OB associations, and of young associations, plotted logarithmically with observed H I density.*

(ii) The youngest associations have a distribution of the form:

$$(\sigma_{OB}) \propto (\sigma_{H\,I})^{1\cdot 73\pm 0\cdot 08}$$

which is closer to that found for H II regions

$$(\sigma_{H\,II} \propto \sigma_{H\,I}{}^{2\cdot 23\pm 0\cdot 11})$$

than is found for older associations. This agrees with a similar result based on the density of high luminosity stars in the Magellanic Clouds (Sanduleak 1969), i.e. $\sigma_{stars} \propto \sigma_{H\,I}{}^{1\cdot 84\pm 0\cdot 14}$ and also with indirect evidence (Schmidt 1959) that in our own galaxy the rate of star formation varies as the square of the gas density.

(iii) There is no significant correlation of H I with the oldest OB associations, nor with those unclassified according to age by van den Bergh.

This relationship between the age of the OB associations and the density of H I cannot be explained by statistical errors, but it is highly probable that a selection effect in the observed distribution of OB associations is present. High H I densities are found in regions with prominent dust features where optical obscuration is high. Older stellar associations consist of fainter stars; hence older associations are more likely to be obscured by dust and to escape detection in regions of high H I density, than are younger, brighter associations. There is in fact a deficiency of older associations observed in regions of high H I density.

Taking account of this selection effect, the following explanations are consistent with the observations:

(i) During the life-time of the older associations, H I in their neighbourhood has been partly consumed in the creation of H II regions, molecular hydrogen, and stars.

(ii) There has been a displacement of older stars with respect to the regions of high H I densities where they were born. This could be either a systematic displacement, due to gravitational perturbations for example, or merely a dispersion in all directions. Displacements of the order of 500 pc in a time of $\sim 3 \times 10^7$ yr are required, corresponding to velocity differences of ~ 15 km s^{-1}. This value is similar to the observed expansion velocities of OB associations and would explain the spread of old associations into regions of lower H I density but not the complete absence of any old associations in regions of high H I density. The density-wave model of spiral structure predicts migration velocities of a similar magnitude; discussion of the H I velocity field in M31 and its relation to the density-wave theory will be discussed in Paper II.

It should be noted that the mean size, 350 pc, of van den Bergh's ' unclassified ' OB associations is comparable to that of the younger associations (300 pc) suggesting that they should not be classified as ' old ' (mean size 800 pc). It may be that these ' unclassified ' associations represent a different class, less massive and intrinsically less luminous, formed preferentially in regions of lower H I density.

4.4 *H I and the radio continuum distribution*

Fig. 13 shows a contour map of the radio continuum emission at 408 MHz (Pooley 1969) which may be compared with the low resolution H I map of Plate I. Although the beam sizes differ—that for the continuum map was $4' \times 4'$, and that for the H I map $6' \times 9'$—the main features of the distribution are strikingly similar. Two features in particular are common to both maps:

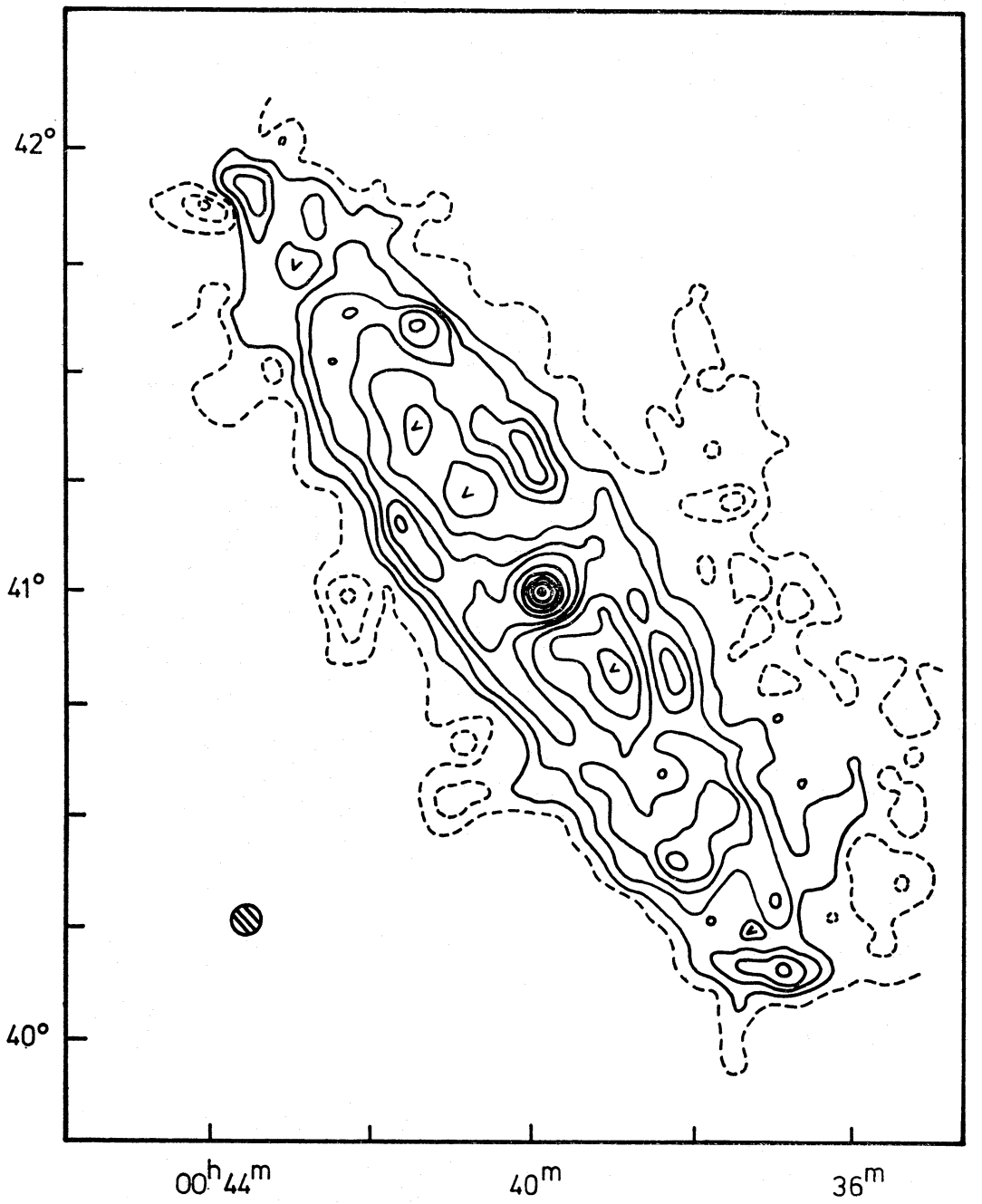

FIG. 13. *The 408 MHz continuum emission from M31 (Pooley 1969). The contour interval is 3 K, and the 4′ beam is shown shaded.*

(i) the central deficiency of both H I and continuum emission within ~15′ of the nucleus (ignoring the strong unresolved continuum source at the nucleus, which has no counterpart in H I); and

(ii) the relative intensities of H I and radio continuum along the ring of emission; where there is a peak of H I there tends also to be a similar peak of radio continuum emission.

Pooley derived the continuum map of Fig. 13 by smoothing observations initially having an angular resolution of 80″ arc. In the original data, kindly made available by him, the noise level is naturally higher but there are continuum

features which correlate well on scales of a few hundred parsecs with both the H I and dust (Plate III). The continuum radiation from the arms of M31 was attributed by Pooley to relativistic electrons from Type II supernovae, and/or to enhanced magnetic fields in the arms; this enhancement might arise from compression of the magnetic field along with the gas, caused for example by a shock wave. The close relationship between H I and radio continuum emission in M31 supports such a model; a similar discussion has been made for M51 by Mathewson, van der Kruit & Brouw (1972). As is discussed by Pooley for M31, and Mathewson *et al.* for M51, the continuum radiation is unlikely to be due to the integrated emission from supernova remnants; if the average rate of formation of these remnants is one every 50 yr (Katgert & Oort 1967) an implausibly long lifetime of 10^6 yr for each would be required to account for the observed radiation.

The comparisons made in this Section between H I, dust, H II regions, OB associations and radio continuum emission show the relationship between H I and other Population I material more clearly than has been possible hitherto in any spiral galaxy other than our own.

5. THE COMPANION GALAXIES

5.1 *M32 and NGC 205*

No H I emission was found in the direction of either of M32 or NGC 205. Upper limits for the H I mass in each galaxy may be estimated by assuming that the H I emission comes from either (i) an area comparable to the optical dimensions, or (ii) unresolved features within the galaxy. The corresponding limits are given below; the figures in brackets are the best values available hitherto (Guibert 1973).

M32: ($8 \times 10^6\ M_\odot$)
(i) $M_{\mathrm{H\,I}} < 1{\cdot}5 \times 10^6\ M_\odot$ (optical dimensions)
(ii) $M_{\mathrm{H\,I}} < 6 \times 10^5\ M_\odot$ (scale size $< 1\frac{1}{2}' \times 2'$)

NGC 205: ($4{\cdot}9 \times 10^6\ M_\odot$)
(i) $M_{\mathrm{H\,I}} < 4 \times 10^6\ M_\odot$ (optical dimensions)
(ii) $M_{\mathrm{H\,I}} < 1{\cdot}6 \times 10^6\ M_\odot$ (scale size $< 1\frac{1}{2}' \times 2'$).

Hodge (1972) has already set a more stringent limit by his estimate that the Population I mass is $5 \times 10^5\ M_\odot$ in NGC 205.

Richstone & Sargent (1972) have estimated the total mass of M32 as $(1{\cdot}3 \pm 0{\cdot}5) \times 10^9\ M_\odot$. The upper limit of H I content is then 0·1 per cent of this mass. Upper limits to the ratio $M_{\mathrm{H\,I}}/M_{\mathrm{Total}}$ are available for a number of other elliptical galaxies and recent values range from 0·1 per cent to less than 0·02 per cent (Gallagher 1972; Bottinelli, Gouguenheim & Heidmann 1973).

The upper limits of H I masses given here are at the 2 σ level of significance; they are based on the assumption that the velocity range of any H I emission from either companion is not greater than 200 km s^{-1}, which is at least twice the optical dispersion measured in M32 (Burbidge, Burbidge & Fish 1961; Richstone & Sargent 1972).

5.2 *The van den Bergh Companion IV*

Van den Bergh (1971, 1972) has discovered four possible new companion

galaxies of M31, one of which (' Andromeda IV ') is smaller, bluer and of a higher surface brightness than the others and lies less than 1° south of the nucleus of M31. He suggested that it might be either a background dwarf galaxy or else a relatively old star cloud in the outer disc of M31.

Fig. 14 shows a map of the integrated H I emission around Andromeda IV, whose position is marked with a cross. Measured velocities of the H I are also indicated. These velocities, and the extended H I emission almost parallel to the

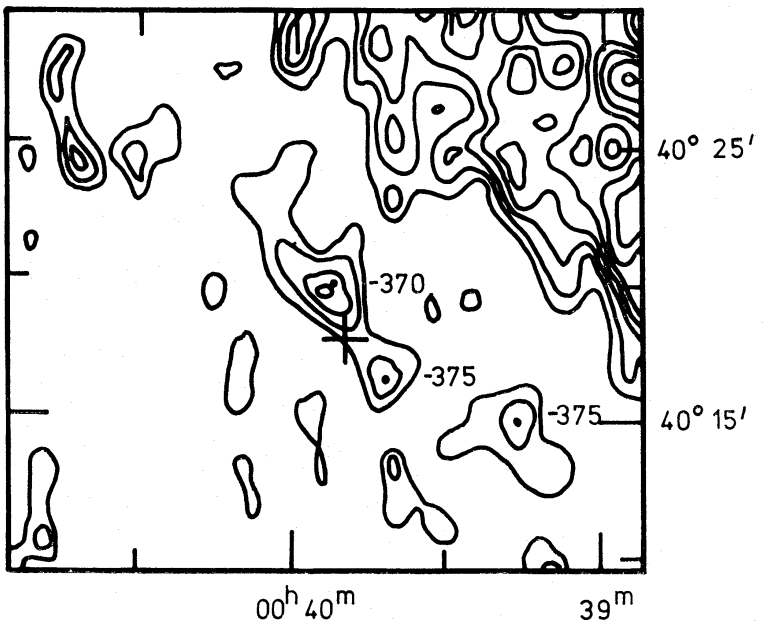

FIG. 14. *Integrated H I emission along part of the SE edge of M31. The position of van den Bergh's ' companion ' Andromeda IV is marked with a cross. The contour interval is 200 K km s^{-1}, zero and negative contours being omitted. Three spot velocity measurements are also shown, in km s^{-1}.*

major axis of M31, suggest strongly that Andromeda IV is indeed associated with M31 and lies in an outer arm which can be traced in H I. If we assume that this ' companion ' lies in the plane of M31, its distance from the nucleus is ≈ 23 kpc. The radial velocity of the H I is (375 ± 5) km s^{-1}, which corresponds to a rotational velocity around the nucleus of (203 ± 14) km s^{-1} if the systemic velocity of M31 is taken as -300 km s^{-1}. This is in good agreement with values of (220 ± 5) km s^{-1} obtained at this distance from the rotation curve on the major axis. Further evidence of the association of this ' companion ' with H I in M31 is given by the fact that, on a scale of ~ 1 kpc, it lies in one of the most intense regions of H I emission along this outer arm. The association with H I may suggest that these stars are in fact relatively young; their appearance may be affected by obscuration caused by dust associated with the H I. It seems likely that similar faint stars may be found elsewhere along this outer arm.

6. CONCLUSIONS

The main conclusions to be drawn from this paper are as follows:

(i) The H I exists in long straggling segments, and provides a spiral arm tracer at least as well defined as optical objects, largely avoiding problems of extinction;

corrections for a finite optical depth in the H I are unlikely to exceed ~30 per cent.

(ii) Peak brightness temperatures observed in the 39 km s^{-1} bandwidth are ≈60 K. Peak values of integrated H I emission observed are ≈3600 K km s^{-1}, or ≈ 14×10^{20} atom cm^{-2} surface density allowing for the inclination of M31. If the H I distribution is assumed to be ~250 pc thick, this represents a true density of 1·8 atom cm^{-3}, comparable to values in the neighbourhood of the Sun in our own Galaxy.

(iii) There is strong correlation, on a scale of a few hundred parsecs, of H I with dust and with radio continuum emission at 408 MHz.

(iv) There is good general agreement, on a scale of ~1 kpc, between peaks of H I emission, and clusters of H II regions. A possible anticorrelation on the scale of a few hundred parsecs may be due to a selection effect in the optical data.

(v) There is a strong correlation of H I surface densities and surface densities of young OB stars. There is, however, no significant correlation for old OB stars or for associations of faint OB stars; this may be partly due to a selection effect in the optical data.

The velocity field of the neutral hydrogen in M31 will be described and discussed in the succeeding paper; particular reference will be made to current theories of spiral structure.

ACKNOWLEDGMENTS

Thanks are due to many members of the Radioastronomy Group for assistance with the observations and data analysis, and in particular to Dr J. E. Baldwin. Helpful comments on the manuscript were received from Dr J. R. Shakeshaft. Financial support from the Science Research Council is also gratefully acknowledged.

Mullard Radio Astronomy Observatory, Cavendish Laboratory, Cambridge

REFERENCES

Argyle, E., 1965. *Astrophys. J.*, **141**, 750.
Arp, H., 1964. *Astrophys. J.*, **139**, 1045.
Baade, W. & Arp, H., 1964. *Astrophys. J.*, **139**, 1027.
Baldwin, J. E., Field, C., Warner, P. J. & Wright, M. C. H., 1971. *Mon. Not. R. astr. Soc.*, **154**, 445.
Bottinelli, L., Gouguenheim, L. & Heidmann, J., 1973. *Astr. Astrophys.*, **25**, 451.
Burbidge, E. M., Burbidge, G. R. & Fish, R. A., 1961. *Astrophys. J.*, **133**, 393 and 1092.
Burke, B. F., Turner, K. C. & Tuve, M. A., 1963. Annual Report, p. 289, Department of Terrestrial Magnetism, Carnegie Institute, Washington, D.C.
Burke, B. F., Turner, K. C. & Tuve, M. A., 1964. The Galaxy and the Magellanic Clouds, *IAU Symposium No.* 20, p. 183.
Davies, R. D. & Gottesman, S. T., 1970. *Mon. Not. R. astr. Soc.*, **149**, 237.
de Vaucouleurs, G., 1958. *Astrophys. J.*, **128**, 465.
Emerson, D. T., 1972. *Proceedings of the First European Astronomical Meeting*, Vol. 3, Galaxies and relativistic astrophysics, Springer-Verlag, Berlin.
Emerson, D. T., 1973. *Ph.D. thesis*, University of Cambridge.
Emerson, D. T. & Baldwin, J. E., 1973. *Mon. Not. R. astr. Soc.*, **165**, 9P.
Gallagher, J. S., 1972. *Astr. J.*, **77**, 7.
Guibert, J., 1973. *Astr. Astrophys.*, **29**, 335.
Guibert, J., 1974. *Astr. Astrophys.*, **30**, 353.
Hartwick, F. D. A., 1971. *Astrophys. J.*, **163**, 431.

Hodge, P. W., 1972. External galaxies and quasi-stellar objects, *IAU Symposium No.* 44, p. 46.
Katgert, P. & Oort, J. H., 1967. *Bull. astr. Inst. Netherl.*, **19,** 239.
Mathewson, D. S., van der Kruit, P. C. & Brouw, W. C., 1972. *Astr. Astrophys.*, **17,** 468.
Mezger, P. G., 1969. The spiral structure of our Galaxy, *IAU Symposium No.* 38, p. 108.
Pooley, G. G., 1969. *Mon. Not. R. astr. Soc.*, **144,** 101.
Richstone, D. & Sargent, W. L. W., 1972. *Astrophys. J.*, **176,** 91.
Richter, G. A., 1971. *Astr. Nachr.*, **292,** 275.
Roberts, M. S., 1966. *Astrophys. J.*, **144,** 639.
Sanduleak, M., 1969. *Astrophys. J.*, **74,** 47.
Schmidt, M., 1959. *Astrophys. J.*, **129,** 243.
van den Bergh, S., 1964. *Astrophys. J. Suppl.*, **IX,** 65.
van den Bergh, S., 1971. *IAU Circ. No.* **2366,** 1971.
van den Bergh, S., 1972. *Astrophys. J.*, **171,** L31.
Warner, P. J., Wright, M. C. H. & Baldwin, J. E., 1973. *Mon. Not. R. astr. Soc.*, **163,** 163.
Wright, M. C. H., Warner, P. J. & Baldwin, J. E., 1972. *Mon. Not. R. astr. Soc.*, **155,** 337.